Paper CIT06-0295

OPTIMIZATION OF NATURAL GAS MURAL FLAME BURNERS PERFORMANCE USING BLACK AND WHITE CCD CAMERA IMAGES

Francisco Domingues Alves de Sousa
Instituto de Pesquisas Tecnológicas do Estado de São Paulo – IPT
Cidade Universitária, CEP 05508-901, Saõ Paulo - SP
fdasousa@ ipt.br

Sandro da Silva Aguiar
Braskem - Unidade de Vinílicos – Alagoas

José Carlos Lourenço
Braskem - Unidade de Vinílicos – Alagoas

In this paper a real case study is presented in which three different burner sizes of mural flat flame type were optimized into a test bench, using a technique involving the measurement of boundary variables: gas and air mass flow rates, temperatures and pressures, flue gas composition and the wall radiant emerging power, this one determining the so called radiation zone efficiency. Radiant emerging power was measured from treated images of the wall obtained by CCD cameras, thus allowing to establish comparisons between its values for different operating conditions and finally to determine the optimal ones (those maximizing the emerging power corresponding to a fixed power released by the burner). Application of the adjustments obtained in the bench to the burners installed in two pyrolysis-furnaces, resulted a significant reduction in specific fuel consumption.

Mural flame burners, burner test, burner optimization, still furnace optimization, pyrolisis furnace optimization

1. Introduction

During the last decades considerable amount of work has been applied to improve industrial processes efficiency, mostly on those that intensively use work and heat, frequently involving combustion equipment. The adopted measures has been: to improve equipment insulation, to tight the regulation of steam traps, to recuperate heat from processes streams early wasted, to reduce the air excess in combustion processes and so on. Even though, the industrial processes still remain very inefficient.

To follow obtaining efficiency improvements one needs to apply energy conservation measures that are no longer of quick insight, quantification and implementation. In a word, they require deeper analysis of the involved phenomena. This paper reports just one of these cases.

Still furnaces in refineries and petrochemical plants and large reheating furnaces in rolling sectors of steel plants are equipped with large number of inspirator burners (where gas jet drags the combustion air) that produce flat mural flames over surfaces of refractory walls which then transfer heat, mainly by radiation to the coils inside which the streams to be heated flow, or to the steel plates correspondingly.

Each furnace is frequently equipped with tenths of burners from two or three different sizes which renders their individual optimization, while installed, very difficult or even impossible. In these cases, establishment of adjustments that lead to the best performance must be carried out in an apparatus external to the furnace, in which each burner is installed rendering possible to measure the following parameters:

- Fuel gas mass flow rate, temperature and pressure
- Air mass flow rate, temperature and pressure (not possible to measure when the burner is installed in the real furnace)
- Radiative heat power leaving the refractory wall on which the burner is attached

Formerly it is important to emphasize what means to seek for an optimal operation condition. This optimization involves several aspects like:

- To fit the burner to the power range that it must release, in other words utilizing it within its operational limits. There are two important limits: the stoichiometric one, beyond which the gas jet does not aspirate enough air for completing the combustion reaction and the dynamic one, above which the flame blows-out. During experimental work, these limits were determined just at its beginnings.
- For a determined value of the released power, to increase or maximize the useful fraction (power transferred to the product's main stream)
- For the fuel being used, to reduce or minimize pollutant emission rates, choosing adequate air/fuel ratios.

The radiative power emerging from the wall, which determines the so called radiation zone efficiency can be measured from treated images of the wall obtained by CCD cameras, thus allowing to establish comparisons between its values for different operating conditions and finally the determination of the optimal ones (those maximizing the emerging power corresponding to a fixed power released by the burner).

2. Equipment description

Figure (1) shows one of the furnaces to which this methodology was applied. It is equipped with four rows of burners in each side of the radiation zone, totalizing eighty burners. At its central plane, parallel to the sides that contain the burners, there is a coil built by 6 inches diameter tubes with 32 passages (horizontal tubes) inside which flows the fluid to be heated. The fluid, Ethylene-dichloride (EDC) enters de coil in the liquid phase, being successively evaporated, superheated and finally cracked, resulting the final product, Vinyl chlorine monomer (MVC).
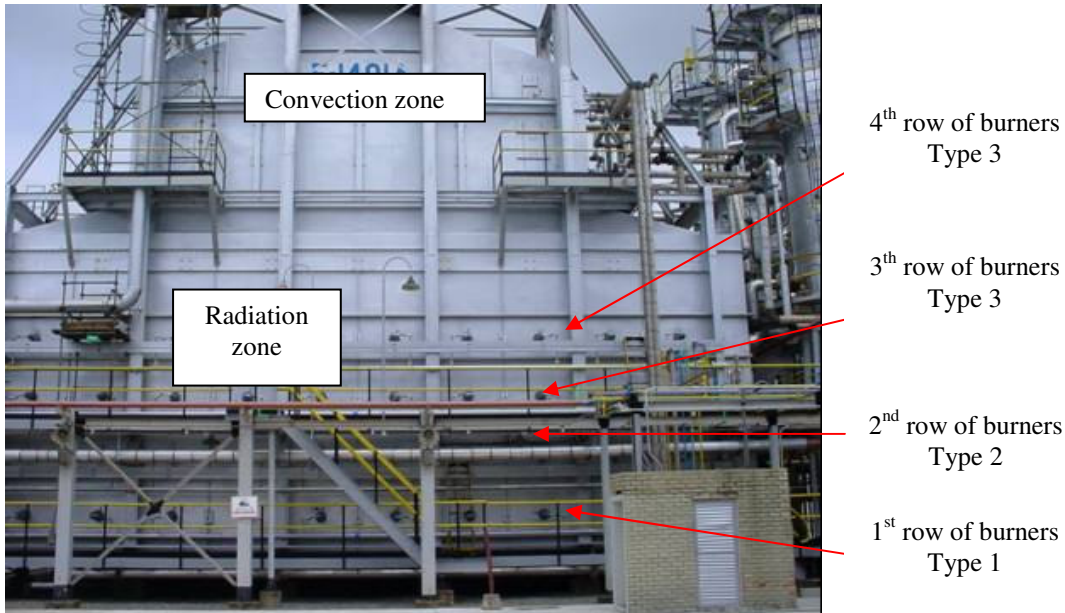
Figure 1 – Cracking furnace with four rows of burners

Figure (2) shows a schematic drawing of the burners and Fig. (3) shows schematically the several heat interactions among the furnace elements
In the present case it is fundamental to optimize $Q_{RAD,WALL,COIL}$ (power exchanged by radiation between the furnace wall and the coil), maximizing $Q_{RAD,FLAME,WALL}$ (power exchanged by radiation between the mural flame and the wall) and $Q_{CONV,FLAME,WALL}$ (power exchanged by convection between the mural flame and the wall).
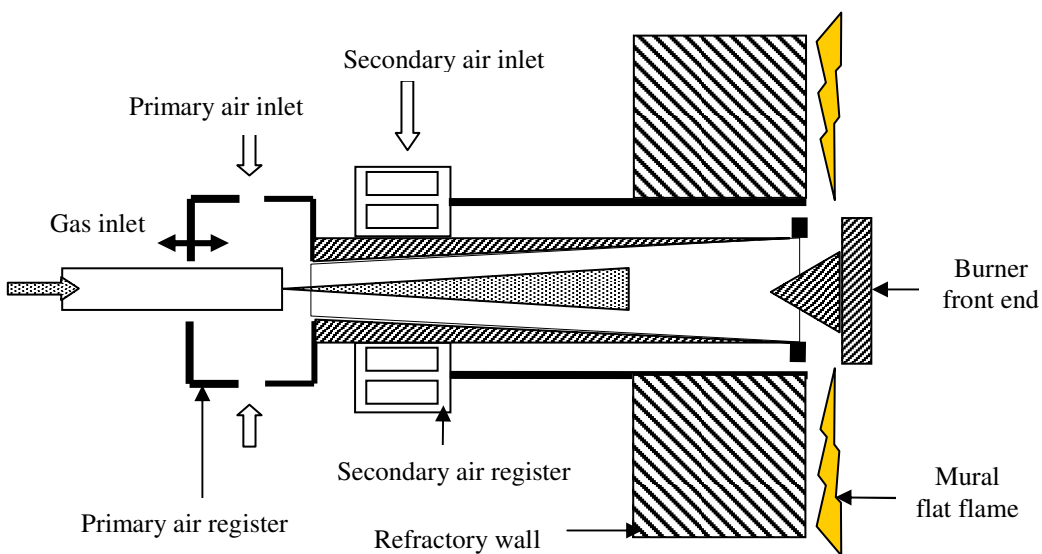
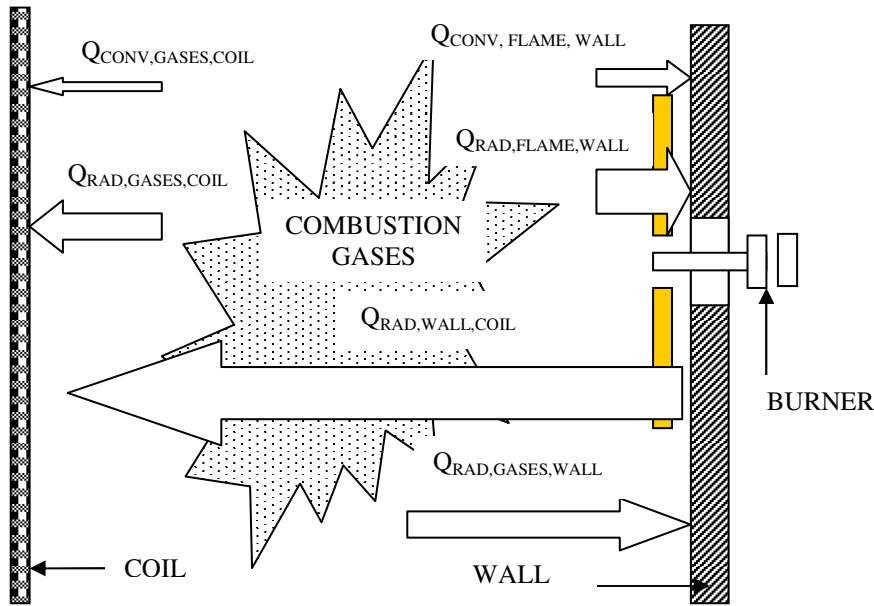Figure 2 – Schematic drawing of the mural type burners

Figure 3 – Heat interactions among furnace elements

3. Laboratory apparatus used for carrying out the trials

3.1. Primary air temperature, pressure and flow rate measurement

For getting information about the performance of each burner it is necessary to measure gas and air flow rates. The last one is practically impossible of being measured given the original configuration of the burners. For this a plenum was built around the air register, provided with a grate that regularizes air entrance across it. Air supplied by one blower passes through a measurement system composed by an orifice plate and pressure transducers before entering the plenum. A valve allows the flow rate adjustment, while maintaining the pressure inside the plenum at zero value to simulate the aspiration of atmospheric air that occurs in a real operation. Resuming, the blower is used only to overcome the pressure drop across the flow rate measurement device.

Figures (4) shows the plenum and the gas plus air supply and measurement system. Figure (5) A and B show the combustion chamber inside just after the burner lightning and at steady state respectively.
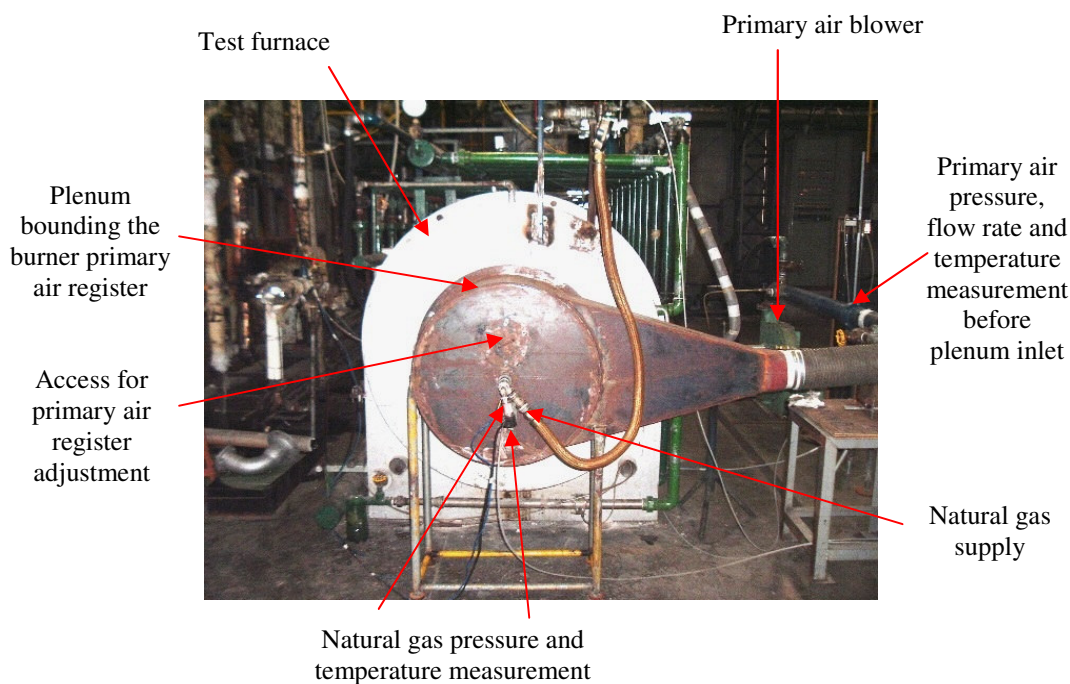

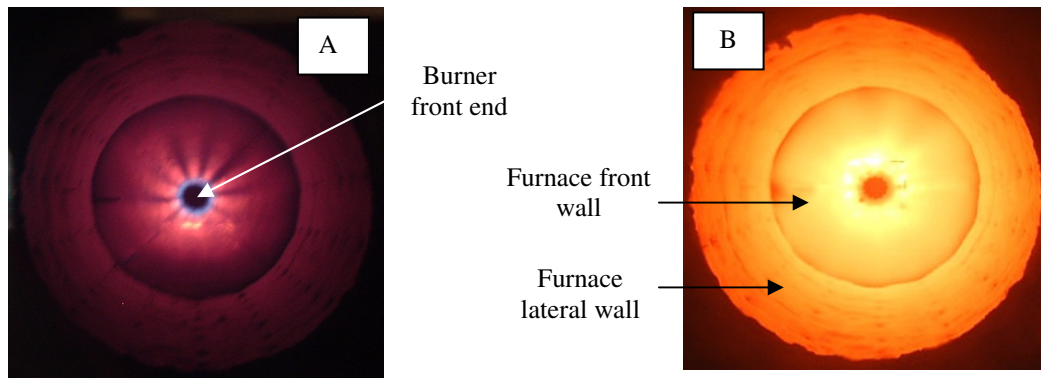Figure 4 – Primary air and natural gas supplying and flow rate measurement

Figure 5 – Pictures of the combustion chamber inside

3.2. Measurement of radiative power emerging from the wall

The technique used in this work for measuring the power emerging from the wall over which the flame develops was the computerized inspection. The images were grabbed by a system composed of the following items:

a) An optical set composed by interference filter (900 nm), made by Corion; 12 mm lens with manual adjustments for focus and <u>obturator</u> , type H12-1.2, made by Rainbow and monochromatic CCD camera, type V-1070, made by Marshall. This set was lodged into a cooled device as shown in Fig. (6). The resulting set was mounted onto the rear part of the furnace flue gases channel, as shown in the right side of the same figure.
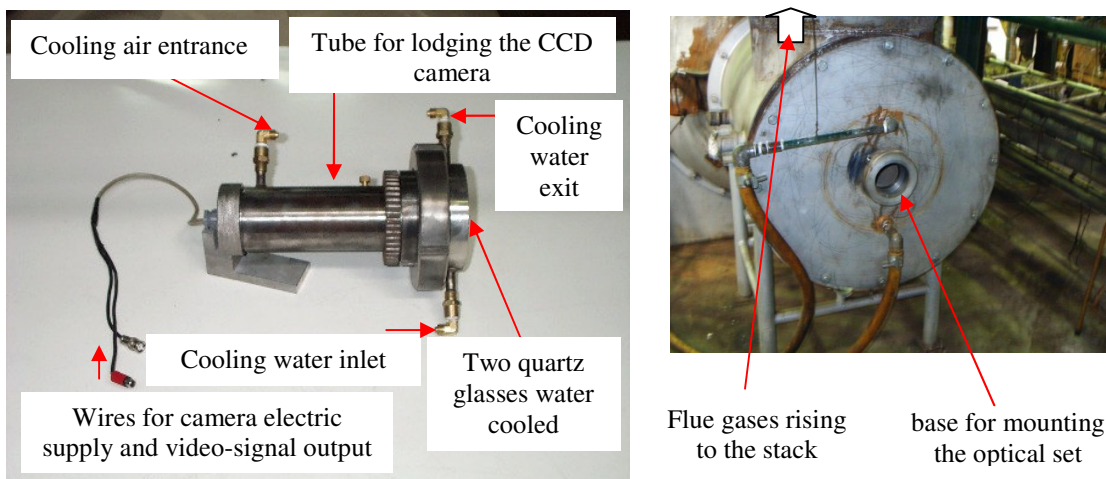

Figure 6 – Optical set mounted on the rear end of the flue gases channel

b) A set of wires for the camera electrical supply and for the signal conduction from it up to the acquisition board which was installed into the computer.

c) The frame acquisition and dispatching board, made by Coreco Imaging.

d) A computer program for automatic visual inspection, called SCIVA, developed by another IPT group, detailed described by Martins (2004), provided with a large tool menu for acquisition, storage in BITMAP file and treatment of images.

3.2.1. Power measurement method validity

A question that certainly one can argue is: if the objective is to shoot images from the internal surface of the furnace front wall where the burner is installed but the optical set is located in the opposed end of the furnace, as shown in Fig. (6), the mural flame interposes between them. As the CO_2 and H_2O (gases that absorb and emit radiation) contents in the flame region and in the resulting combustion gases volume are quite high, radiation intensities that strike the optical system may be different from those emerging from the wall thus the obtained images would not correspond to the real situation, being not comparable as well.

In the present case this is not a problem once both gases do not have emission/absorption bands for wave lengths bellow 1600 nm, as shown in Fig. (7) for CO_2. For steam the lower band is located near the correspondent for CO_2 and the others are located at higher wave lengths. As the radiation crossing the interference filter has wave length close to 900 nm, only this radiation (not intervenient with the combustion gases) strikes the camera sensor device (CCD). This fact validates de calculations presented in item 4.
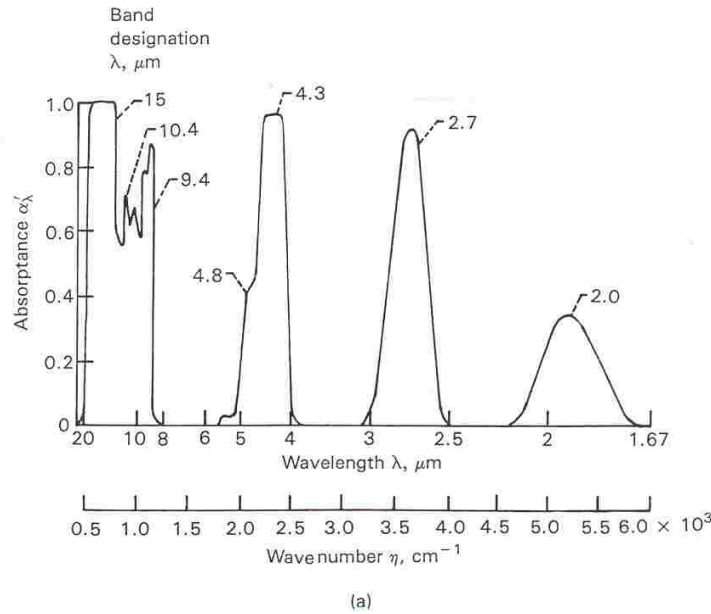
Figure 7 – Emission/absorption bands for CO_2 (Siegel & Howell 1992)

3.2.2. Image comparisons

The black and white images obtained correspond to a wave length narrow range around 900 nm and they have 256 gray tons from black (0) to white (255). Each one of these tons, called *threshold,* is proportional to the radiation intensity emerging from the corresponding point of the front wall internal surface, for the considered wave length. This assumption is detailed discussed by Dewitt and Nutter (1989).

It is important to notice that, inside the proportionality constant there are, among others, the effects by attenuation introduced by the interference filter, by the image grabbing time (lower the exposition time, lower is the power striking onto the CCD), by the opening area of the lens obturator (lower the opening lower is the power striking onto the CCD) and the effect of wall emissivity.

The grabbing time is inversely proportional to the acquisition frequency that can be: 60 s^{-1}, 125, 250, 500, 1000, 2000, 4000 and 10000 s^{-1}, depending on the shutter adjustment, for the camera used.

In this work all images were made with the higher frequency to avoid the saturation of large fraction areas in the images (these areas become completely white, despite their different temperatures, if lower frequencies are used). The obturator was adjusted in a previous experiment also to avoid the saturation.

Obviously the comparisons between images that will be done lately are only valid if the interference filter, the camera, the image acquisition frequency, the lens and the obturator adjustment are the same as well as the emissivity of the surface being observed. Each image is composed by 307200 pixels distributed into 480 rows and 640 columns, having a *threshold* comprised between the before mentioned limits.

4. Calculation procedure

Beforehand it is important to notice that this procedure is not a novelty; in fact a procedure, utilizing image acquisition equipment similar to the present one and part of the assumptions made here, was used by Huang (2000) for calculating the temperature distribution in flames inside a test furnace.

Each elemental area of the wall internal surface emits radiation for all directions of a semi-space, as shown schematically in Fig. (8).
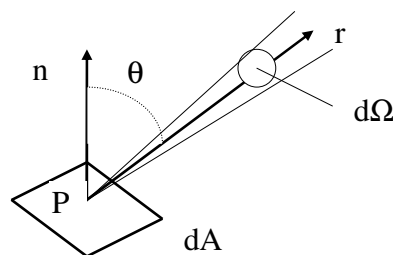

Figure 8 – Radiation emerging from an elemental area, around direction r

The power emerging from dA, inside the solid angle dΩ, centered into the direction r, with vertice at the point P, with wave length λ, called $d^2 q_\lambda$, may be expressed as:

$$d^2 q_\lambda = I_{\lambda,r} * dA * \cos\theta * d\Omega \tag{1}$$

Thus the radiative power emerging from dA to all the directions of the semi-space may be calculated as:

$$dq_\lambda = \int_{\Omega=2\pi} I_{\lambda,r} * dA * \cos\theta * d\Omega \tag{2}$$

The radiative power emerging from an area at the wall surface is then:

$$q_\lambda = \int_A dq_\lambda \tag{3}$$

As long as some assumption is made about the $I_{\lambda,r}$ directional variation the integral in Eq.(2) involves only geometry. If one admits that $I_{\lambda,r}$ is constant for all directions (isotropic emission) then it can be took outside the integral and it is straight to conclude that dq_λ is proportional to $I_{\lambda,r}$.

Considering that the *threshold* of each pixel is proportional to $I_{\lambda,r}$ of the corresponding point in the wall surface, one can conclude that the power emerging from each elemental area is proportional to its image's corresponding pixel. This conclusion will be extensively used when comparing the images obtained. Additionally the assumption that the wall internal surface is gray is equivalent to impose that the emerging radiation intensity from each of its points, at the wave length λ is proportional to the blackbody one at the same wave length.

$$I_\lambda = \varepsilon * I_{\lambda,b} \tag{4}$$

Where I_λ is the emerging radiation intensity of the wall surface (with emissivity ε) and $I_{\lambda,b}$ is the blackbody spectral intensity at the same temperature, expressed by the Planck equation.

$$I_{\lambda,b}(\lambda,T) = \frac{2 * C_1}{\lambda^5 * (e^{C_2/\lambda*T} - 1)} \tag{5}$$

Where
C_1 = first Planck constant (0,59552197*10^{-16} W.m^2/sr)
C_2 = second Planck constant (0,01438769 m*K)
λ = wave length [m]
T = absolute temperature [K]

Thus the gray tons distribution also allows to immediately verifying the temperature distribution on the internal wall surface (contacting the mural flame). As closer to the white, the higher the *threshold*, the higher is the temperature of the corresponding region.

As long as this brief conceptual introduction is made one considers two typical images obtained during the burners hot tests. The interest is to compare both under two aspects: wall surface temperature uniformity and power emerging from them (at the wave length λ = 900 nm)

Higher or lower temperature uniformity may be quantified by the application of a tool existing in the program SCIVA, called histogram.

The emerging power from a selected region in the wall, around the burner quarl can be quantified as described on the following, using two images corresponding to two different tests (means of 3600 instant images). Due to space limitations the procedure will be applied to two tests carried out with the type 2 burner for verifying the effect of the air excess on these emerging powers. Tests where numbered as 6B (air excess around 20%) and 6C (air excess around 5%). The mean global images are shown in Fig. (9).

These images show the inner surface of the flue gases channel and the lateral surface of the furnace. In fact, the interest for this work is to compare only the central circle corresponding to the wall in which the burner is mounted and whose front end appears as black (low temperature) in the center of the circle.

For this the program is provided by a tool that allows to separate a definite region, for instance by the squares (in white) in Fig. (9). The sub-images are shown in Fig. (10) (left sides).

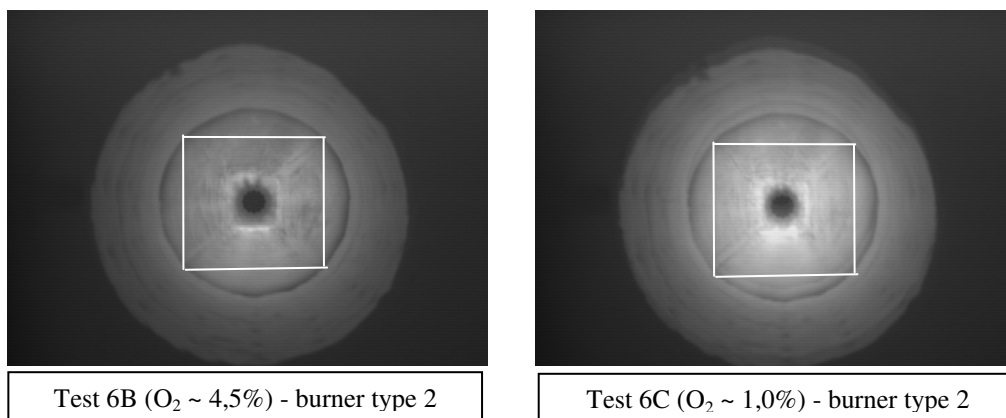| Test 6B (O$_2$ ~ 4,5%) - burner type 2 | Test 6C (O$_2$ ~ 1,0%) - burner type 2 |

Figure 9 – Mean global images – Tests 6B and 6C – burner type 2

The inspection of these images allows the immediate conclusion that the wall temperature uniformity in the test 6C is slightly worse than that of the test 6B. This quality may be better expressed by the application of the histogram to these sub-images. Its horizontal axis refers to the *thresholds* and over the ordinate axis the heights are proportional to the number of pixels in that *threshold*. The histograms corresponding to those sub-images are shown in Fig. (11) (right).

The inspection of the histograms allows the conclusion that in the test 6C there exist regions on the wall emitting radiation in a broader range of intensities (the base of its histogram – threshold values - is larger) compared to the test 6B.

On the sub-images of Fig. (10) it can be applied another tool, existing into the program SCIVA, called THRESHOLDING. Briefly, given a definite threshold I, this tool applied to an image does the following: assigns value 0 (zero) to all the pixels which threshold is lower than I and value 255 to all the pixels which threshold is higher than I, generating thresholded images as shown in Fig. (11). These images are just an example, they do not correspond to those of Fig. (10).

For each thresholded image it is possible, using another tool from SCIVA, to calculate the white part area – set of pixels which threshold value is higher than that indicated in the label. For instance, referring to the threshold value I$_1$ one can calculate the areas A$_{LIMI1}$ for both the tests 6B and 6C; for the threshold value I$_2$ the process can be repeated and so on. For each initial sub-image one can calculate the difference (A$_{LIMI1}$ - A$_{LIMI2}$) which represents an area (part of the sub-image) corresponding to a emerging radiation intensity comprised between I$_{1,\lambda}$ and I$_{2,\lambda}$ (thresholds I$_1$ e I$_2$).

As was seen early, power emerging from the wall region corresponding to (A$_{LIMI1}$ - A$_{LIMI2}$) can be calculated as:

$$q_{(ALIM1-ALIM2)} = K*(A_{LIM1} - A_{LIM2})*THRE_{MEAN,1-2}$$ (6)

Where THRE$_{MEAN,1-2}$ is a mean value between I$_1$ and I$_2$ and K is the proportionality constant (see item 3.2.2).
Eq. (6) is a discretized form of the Eq. (3).

| Sub-image | histogram | Sub-image | histogram |

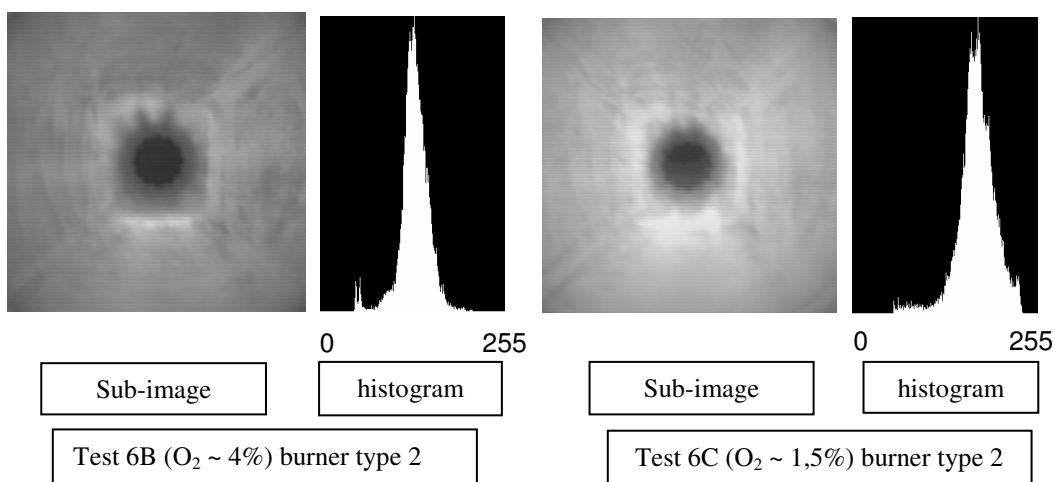| Test 6B (O$_2$ ~ 4%) burner type 2 | Test 6C (O$_2$ ~ 1,5%) burner type 2 |

Figure 10 – Sub-images and histograms – Tests 6B and 6C – burner type 2
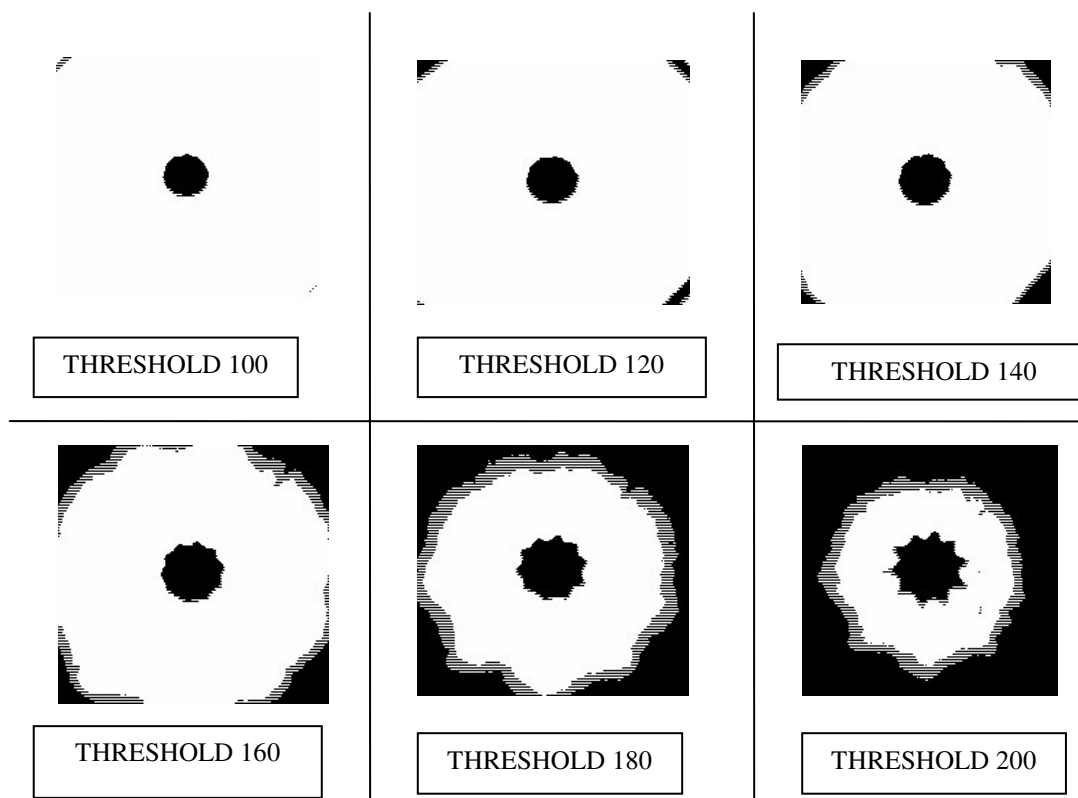
Figure 11 – Appearance of a sub-image after thresholding

Table 1 presents, in a condensed form, the values calculated for the tests 6B and 6C. The values SOMA(d(AREA) * THRE$_{MEAN}$) are proportional to the emerging powers from the regions inside the squares (sub-areas) of Fig. (10) for the corresponding tests. It is important to notice that these last values are expressed in arbitrary units.

Areas of the thresholded images, A$_{LIMi}$, from the table are represented into Fig.(12), being straightforward to conclude that the area under the red curve (corresponding to test 6C), which is equivalent to **SOMA(d(AREA) * THRE$_{MEAN}$)**, is considerably higher than that under the blue curve (corresponding to test 6B). In this figure it is possible to appreciate the internal surface wall temperature uniformity. If the curve presents, in its initial region, small values of (d(AREA)/d(THRE)), the uniformity is high and vice-versa. In the tests being shown the uniformity is lower in both cases.

Table 1 – Effect of the air excess on the wall emerging power – burner type 2

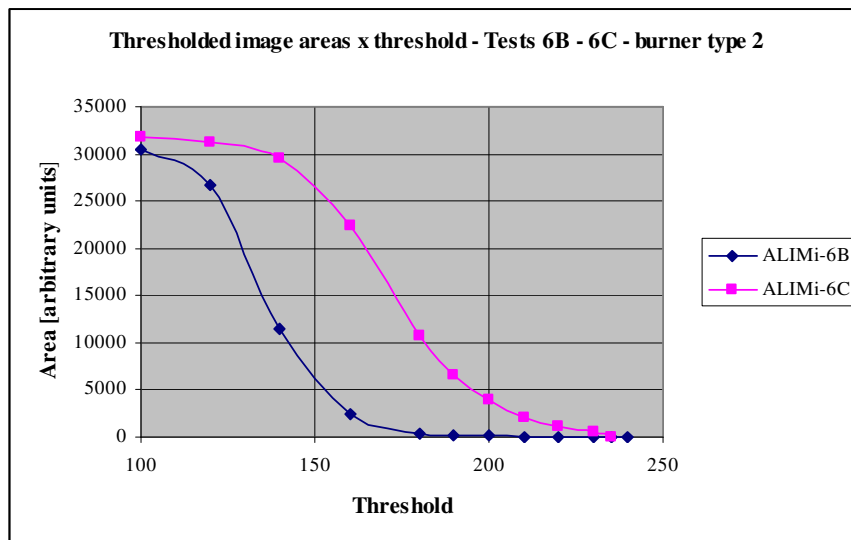| TEST 6B – BURNER TYPE 2					TEST 6C – BURNER TYPE 2				
HIGH AIR EXCESS (4,5% O2)					LOW AIR EXCESS (1% O2)				
THRE	A$_{LIMi}$	d(AREA)	THRE$_{MEAN}$	THRE$_{MEAN}$ x d(AREA)	THRE	A$_{LIMi}$	d(AREA)	THRE$_{MEAN}$	THRE$_{MEAN}$ x d(AREA)
100	30410	3765	110	414150	100	31893	654	110	71940
120	26645	15216	130	1978080	120	31239	1720	130	223600
140	11429	8911	150	1336650	140	29519	7104	150	1065600
160	2518	2126	170	361420	160	22415	11712	170	1991040
180	392	195	185	36075	180	10703	4081	185	754985
190	197	92	195	17940	190	6622	2745	195	535275
200	105	71	205	14555	200	3877	1725	205	353625
210	34	31	215	6665	210	2152	967	215	207905
220	3	3	225	675	220	1185	607	225	136575
230	0	0	232,5	0	230	578	578	232,5	134385
235	0	0	237,5	0	235	0	0	237,5	0
240	0				240				
SOMA(d(AREA) * THRE$_{MEAN}$)				**4166210**	SOMA(d(AREA) * THRE$_{MEAN}$)				**5474930**
DIFFERENCE RELATED TO THE LOWER VALUE (%)									**31,4**

Figure 12 – Thresholded image areas – tests 6B and 6C – burner type 2

5. Additional aspects studied by means of images

Beyond the air excess effect, shown in item 4 for the case of type 2 burner, the following additional features were verified:

- Effect of the type 2 burner operation above its upper stoichiometric limit
- Effect of the substitution of type 2 burners by type 1 burners
- Effect of excessive gas jet momentum for the type 3 burners

5.1. Effect of operating the burner above its stoichiometric limit

During the preliminary tests it was verified that the upper stoichiometric limit for the type 2 burner was 17,8 kg/h, which corresponds to the natural gas pressure (P_{GN} = 2,6 kgf/cm^2 gauge) ahead the injector nozzle. Nevertheless in each extremity of rows 3 and 4 of the furnace one burner of this burner type was originally installed, operating at gas pressures P_{GN} = 3,4 kgf/cm^2, corresponding to a flow rate of 22,4 kg/h and these burners often presented stability problems. By this motive the burner was operated in the test furnace at both described conditions. At the higher throughput additional air was supplied externally to the burner body, simulating the real furnace operation.

The results of the tests 7A (stoichiometric limit) and 7B (above stoichiometric with tertiary air supply) show clearly the harm derived from this. In fact the power supplied to the burner in the test 7B was 25,8% higher than that supplied in the test 7A, but the emerging power from the wall had an improvement of only 9,5% as shown by a calculation similar to that explained in item 4. The wall sub-images for these tests are shown in Fig. (13) and the thresholded areas versus thresholds are shown in Fig. (14).

Figure 13 – Wall sub-images – tests 7A (left) and 7B (right) –burner type 2
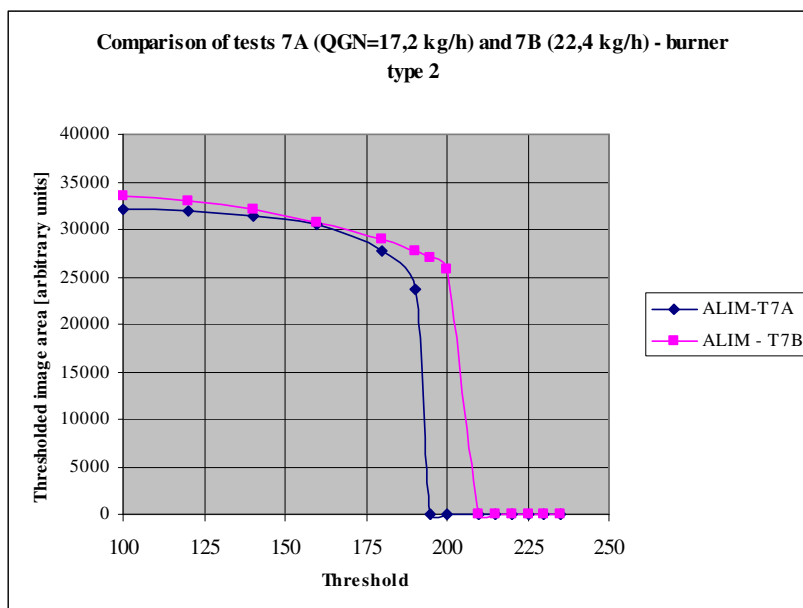
Figure 14 - Thresholded image areas – tests 7A and 7B – burner type 2

5.2. Replacement of type 2 burners by those of type 1

The bare visual inspection of the three burner models made at the work beginnings show clearly that the divergent throats and the outlet areas of the burner types 1 and 3 had been well designed but the same had not occurred for the type 2 (it clearly seems an improvisation). In fact the performance of that burner model was worse under several aspects (operation limits – dynamic and stoichiometric – and wall emerging power) when compared with the other two.

By this motive a test was carried out in which it was verified that the type 1 burner could replace the type 2, installed at the furnace row 2, with advantages. In this case the existing burners operate at 1,4 kgf/cm^2 gas pressure with 12,0 kg/h gas flow rate. To obtain the same gas flow rate, the type 1 burner would operate with 0,8 kgf/cm^2 gas pressure. The reference test with type 2 was numbered 6A and that carried out with the type 1 was numbered 2A. Both of them were carried out with the same air excess. Fig. 15 shows wall sub-images for the tests.
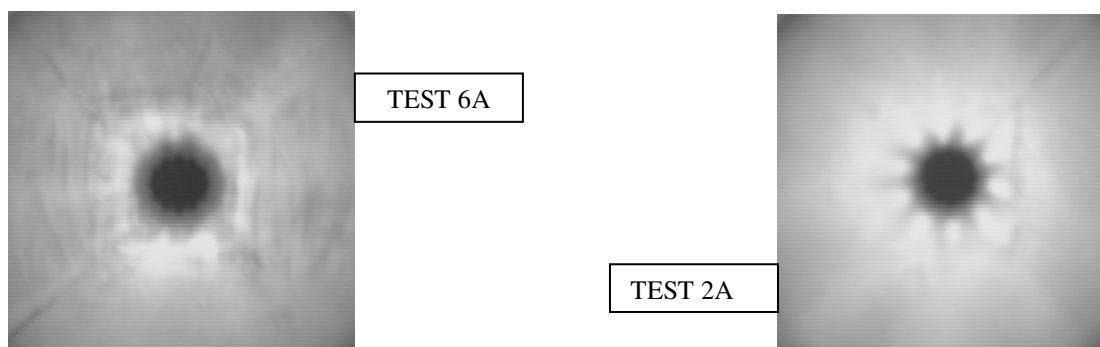

Figure 15 – Effect of replacing the burner type 2 by the type 1 on the refractory wall thresholds

These images show clearly the improvement on the emerging power when the burner type 1 is operated at the same conditions of the burner type 2. Fig. (16) quantifies this qualitative impression.

Using the calculation procedure presented in table 1 it is possible to conclude that the proposed replacement implies an increase of almost 17% on wall's emerging radiative power.
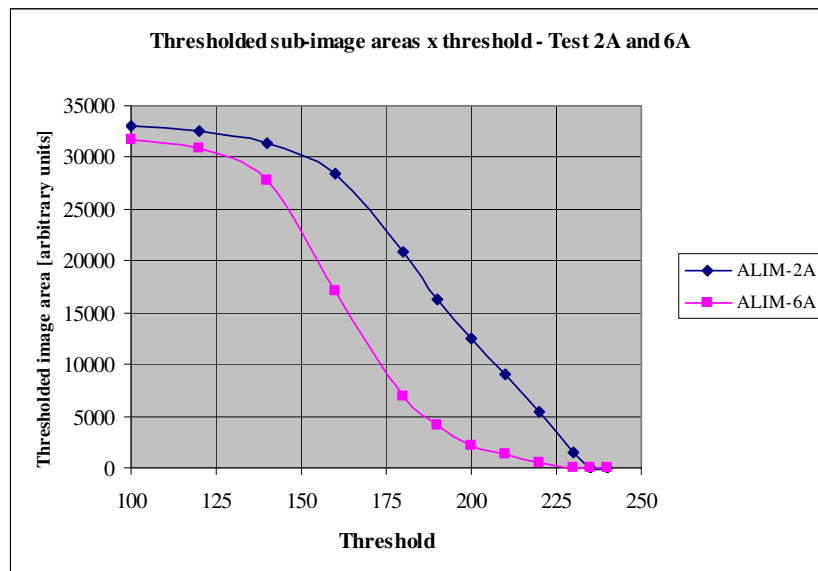
Figura 16 - Effect of the replacement of burner type 2 by the type 1 on the areas of the thresholded sub-images

5.3. Effect of the excessive momentum of gas jet

During the field work it was verified that type 3 burners installed at the levels 3 and 4, Fig.(1) were operating under the following conditions: PGN = 3,40 kgf/cm^2 (gas flow rate, Q_{GN} = 12,4 kg/h) and with 10 mm openings of the primary air register. The operators reported serious difficulties in their operation mainly related to flame's instability (blow-out).

For that throughput and taking into account the results of the preliminary tests carried out in the test furnace it became clear that the adjustment originally applied implied high air excess and high propensity to flame blow-out. It must be noticed that in the test furnace the primary air register had to be adjusted for 3,0 mm opening (being the secondary register completely closed) in order to achieve O_2 contents in the flue gases between 1,2 and 1,4% (best condition for economy).

This problem is clearly due to the excessive gas jet momentum implying, additionally to a high air trust rate, a non-symmetric exiting velocity profile for the gas-air mixture as shown in Fig. (17), promoting the trust of large low temperature gases into the flame, thus lowering its temperature and hence decreasing $Q_{RAD,FLAME,WALL}$ and $Q_{CONV,FLAME,WALL}$ (see Fig.3).

Due to this problem, a modification was introduced into the gas nozzle consisting in a increasing of its diameter from 2,65 to 3,5 mm. This allowed the gas pressure to be lowered from 3,4 to 1,6 kgf/cm^2 and the primary air register opening to be increased from 3,0 to 10,0 mm, improving its switching. After this the test number 10 was carried whose results are to be compared with those of test 9, made previously the modification, both with the same throughput and same air excess.
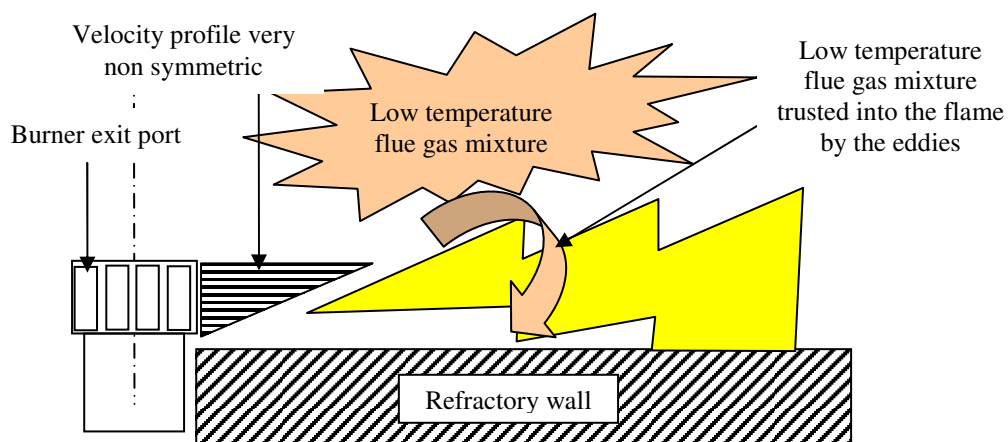

Figure 17 – Effect of excessive gas jet momentum on flame temperature

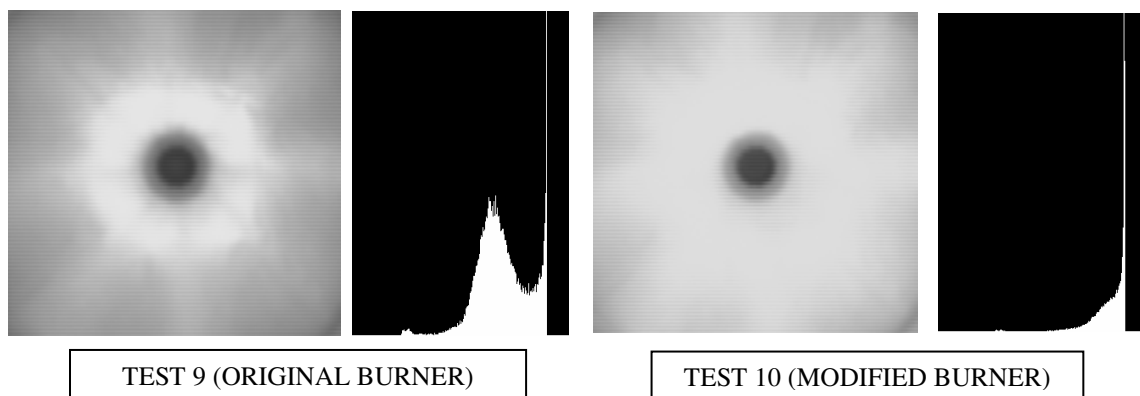| TEST 9 (ORIGINAL BURNER) | TEST 10 (MODIFIED BURNER) |

Figure 18 – Wall sub-images and their histograms - tests 9 and 10 – burner type 3

The bare visual inspection of the Fig.(18) sub-images, allows the conclusion that the temperature uniformity was improved due to the modification done. This is quantified by the histogram area reduction. It must be observed that the uniformity enhancement is an important goal of the work as it contributes to uniformize the heat flux striking the furnace coil. Nevertheless the most important improvement was the increase of wall emerging power, as shown in Fig.(19). The application of the calculation procedure shown in table 1 lead to a power increase of 18%.
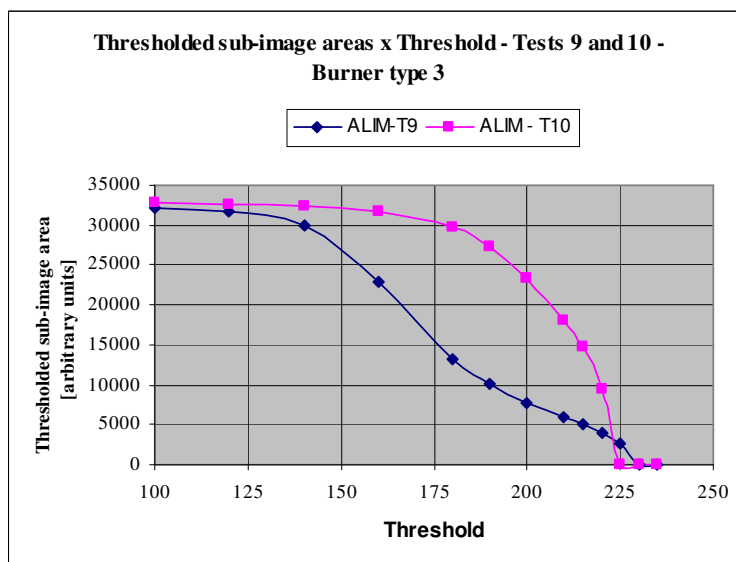

Figure 19 – Effect of the gas jet momentum decrease on the areas of the thresholded wall sub-images – Burner type 3

6. Conclusions

Using the proposed technique it was possible to identify and apply considerable improvements either on the burners operational stability or in the wall temperature uniformity with benefic consequences onto the furnace campaign and additionally to increase substantially the radiation zone efficiency. The application of the recommendations shown in Sousa (2005) to the whole furnace lead to a reduction of natural gas consumption around 15%. Finally it is important to stress that a technologic tool was developed, able to be applied for similar cases.

7. References

Dewitt, D.P. and Nutter, G.D., in: Theory and Practice of Radiation Thermometry, Wiley, New York, 1989.

Huang, Y., Yan, Y. and Riley, G., "Vision-based measurement of temperature distribution in a 500-kW model furnace using the two-colour method". Measurement, 28, pp.175-183, Elsevier Science Ltd.2000.

Martins, F.P.R., Lima, P.S.P., Quiroz, L.H.C., Bruna, W. Almeida, R.Z.H. "Sistema de leitura automática de códigos de licença". In: Brazilian Symposium on Artificial Neural Networks, 2004, São Luis. Proceedings of SBRN 2004, 2004.

Siegel, R. & Howell, J.R., "Thermal Radiation Heat Transfer", Third Edition, Taylor & Francis Inc, 1992.

Sousa, F.D.A. "Modificações em queimadores de fornos petroquímicos visando melhoria de condições operacionais". Technical Report nº 80.070-205 – Instituto de Pesquisas Tecnológicas do Estado de São Paulo – IPT (2005).